Available online at www.sciencedirect.com

SciVerse ScienceDirect

Ceramics International 38 (2012) 6705–6712

CERAMICS INTERNATIONAL

www.elsevier.com/locate/ceramint

Comparison of thermal shock resistances of plasma-sprayed nanostructured and conventional yttria stabilized zirconia thermal barrier coatings

Hossein Jamali*, Reza Mozafarinia, Reza Shoja Razavi, Raheleh Ahmadi-Pidani

Malek-Ashtar University of Technology, Department of Materials Engineering, Shahinshahr, Isfahan, Iran

Received 7 May 2012; received in revised form 20 May 2012; accepted 20 May 2012
Available online 25 May 2012

Abstract

The main goal of the current study is evaluation and comparison of thermal shock behavior of plasma-sprayed nanostructured and conventional yttria stabilized zirconia (YSZ) thermal barrier coatings (TBCs). To this end, the nanostructured and conventional YSZ coatings were deposited by atmospheric plasma spraying (APS) on NiCoCrAlY-coated Inconel 738LC substrates. The thermal shock test was administered by quenching the samples in cold water of temperature 20–25 °C from 950 °C. In order to characterize elastic modulus of plasma-sprayed coatings, the Knoop indentation method was employed. Microstructural evaluation, elemental analysis, and phase analysis were performed using scanning electron microscopy (SEM), energy dispersive spectroscopy (EDS), and X-ray diffractometry (XRD) respectively. The results revealed that failures of both nanostructured and conventional TBCs were due to the spallation of ceramic top coat. Thermal stresses caused by mismatch of thermal expansion coefficients between the ceramic top coat and the underlying metallic components were recognized as the major factor of TBC failure. However, the nanostructured TBC, due to bimodal unique microstructure, presented an average thermal cycling lifetime that was approximately 1.5 times higher than that of the conventional TBC.

Keywords: Nanostructured thermal barrier coating; Yttria stabilized zirconia; Thermal shock; Atmospheric plasma spraying

1. Introduction

Increased operating temperatures and hence, improved performance of gas turbines or diesel engines can be realized by using thermal barrier coatings (TBCs) [1–6]. A typical TBC system consists of a metallic bond coat and a ceramic top coat. The bond coat (PtAl or MCrAlY, M = Ni and Co) protects the substrates from oxidation and improves the adhesion of the ceramic top coat to the metallic substrate. The ceramic top coat has a significantly low thermal conductivity and reduces the temperature of the underlying superalloy in relation to the gas path temperature [7–11]. Yttria stabilized zirconia (YSZ) is the current industrial standard material of TBCs, owing to its low thermal conductivity, phase stability at relatively high temperatures, a relatively high coefficient of thermal expansion (CTE), and chemical inertness in combustion atmospheres as compared to other ceramics [12–15]. Nowadays, TBCs are usually produced by either atmospheric plasma spraying (APS) or electron beam-physical vapor deposition (EB-PVD) [16–18]. However, due to the comparatively cost-effective deposition conditions and high deposition efficiency, plasma spraying technology has enjoyed widespread acceptance up to now [3,19].

Due to a high demand for high-temperature operation of gas turbines, an advanced TBC is essential to improve the performance of gas turbines. Creation of nano-structures is a promising approach to fabricate novel TBCs. In recent years, the nanostructured zirconia based TBCs deposited by atmospheric plasma spraying have been the focus of attention. It was reported that nanostructured thermal barrier coatings had high bonding strength [20], low thermal conductivity [20–24], and prolonged thermal

*Corresponding author. Tel.: +98 312 5232090; fax: +98 312 5228530.
E-mail address: h.jamali@mut-es.ac.ir (H. Jamali).

0272-8842/$36.00
http://dx.doi.org/10.1016/j.ceramint.2012.05.060

cycling lifetime [25–27]. Accordingly, nanostructured TBCs are expected to provide better performance than the conventional TBCs. However, in spite of this, few reports on plasma-sprayed nanostructured TBCs have been published. On the other hand, flawless performance of TBCs is a very important subject in the industry. Since contribution of these coatings in turbine engine efficiency is undeniable, their durability against high temperature thermal cycles is very important. Therefore, the purpose of the current study is the investigation and comparison of the thermal shock resistance of plasma-sprayed nanostructured and conventional YSZ TBCs.

2. Experimental procedures

2.1. Materials

Inconel 738LC Ni-based superalloy was used as the substrate material. In the atmospheric plasma spraying process, two kinds of nanostructured and conventional YSZ powders were used as feedstock for the top coat. The nanostructured YSZ powder was Nanox S4007 (Inframat Corp., Farmington, CT). This powder consisted of agglomerated nanosized particles. The conventional YSZ powder was Metco 204NS (Sulzer Metco, Westbury, NY). In addition, the commercially available NiCoCrAlY powder (22 SN 6883, S.N.M.I.-Avignon) was used as a feedstock for the bond coat. The feedstock characteristics of the powders are presented in Table 1.

2.2. Atmospheric plasma spraying

The thermal barrier coatings, composed of a bond coat (125 ± 25 μm thick) and a top coat (265 ± 25 μm thick), were deposited by an atmospheric plasma spraying (APS) system. Atmospheric plasma spraying was carried out by the Plasma-Technik A3000S system (Sulzer Metco, Wohlen, Switzerland) with a F4-MB plasma torch (Sulzer Metco AG, Winterthur, Switzerland). The spraying parameters are presented in Table 2. In order to improve adherence capability between the bond coat and substrate, the substrates were grit-blasted with alumina particles and then washed with acetone. The measured surface roughness (R_a) of substrates was 9.20 μm. During the spraying process, a cooling system (air blowing) was applied to reduce the coating temperature.

2.3. Thermal shock test

Thermal shock test was performed by heating and the water quenching method. The samples were heated at 950 °C for 5 min in an electric furnace (Nabertherm N7/H, Germany), and then they were thrown into cool water quickly. The temperature of the water throughout the cycling was 20–25 °C. When the samples were cooled to the ambient temperature, they were taken out, dried and put into the high temperature furnace again, repeating the same process. More than 10% of the visible destroyed region of the coating surface was adopted as the criterion for the TBC failure (as the thermal cycling lifetime of the coating). The repeatability of the test results was verified by using three test samples in the same way. This type of thermal shock testing has also been performed by other researchers [28–30]. The macroscopic images of the samples in time during the thermal shock test were captured using a digital camera. The weight changes of the samples were measured to a precision of 0.1 mg by an analytical balance (TE214S, Sartorius, Germany).

Table 1
Feedstock characteristics of the powders.

Commercial powder name	Composition (wt%)	Particle size (μm)	Morphology
Nanox S4007	ZrO_2–$7Y_2O_3$	−150+15	Spherical-agglomerated nanostructured
Metco 204NS	ZrO_2–$8Y_2O_3$	−125+11	Spherical
22 SN 6883	Ni–23Co–18Cr–6Al–1Y	−75+38	Spherical

Table 2
Plasma spray parameters.

Parameter	NiCoCrAlY	Conventional YSZ	Nanostructured YSZ
Current (A)	600	600	600
Voltage (V)	75	61	72
Primary gas, Ar (slpm)	65	35	35
Secondary gas, H_2 (slpm)	14	12	10
Carrier gas, Ar (slpm)	2.3	2.6	3.5
Powder feed rate (g/min)	40	40	18
Spray distance (mm)	120	120	120
Nozzle diameter (mm)	6	6	6
Injector diameter (mm)	2.5	1.8	1.8
Injector position	External	External	External

2.4. Coatings characterization

The microstructure of as-sprayed coatings was investigated by a field emission scanning electron microscope (FESEM; S-4160, Hitachi Ltd., Japan). Phase analysis was carried out by X-ray diffractometry (XRD; Bruker D8 Advance diffractometer, Germany) with filtered Cu-Kα radiation (0.15406 nm). In order to cater to microstructural and elemental analyses of samples after thermal shock test, a scanning electron microscope (Seron Technology-AIS-2000, Korea) equipped with an energy dispersive spectrometer (EDS) was used. The surface roughness (R_a) of substrates prior to spraying was measured by a roughness tester (Mitutoyo SJ-201P, Japan).

The Knoop indentation method has been used to determine the elastic modulus (E) of YSZ ceramic coatings. The elastic modulus (GPa) can be estimated by measuring the elastic recovery of the residual surface impression of the indentation diagonals as follows [31–33]:

$$E = \frac{(-\alpha H_K)}{(b'/a' - b/a)} \quad (1)$$

where H_K denotes the Knoop microhardness (Pa), b'/a' refers to the ratio of the short to long indention diagonals after elastic recovery, b/a is the ratio of the known Knoop indenter dimensions or geometry (1/7.11), and α is a constant having a value of 0.45. In this study, the Knoop indentation tests were performed on the polished cross sections of specimens using a microhardness tester (Clemex, HT-2001, Canada). The load used was 1.96 N (200 gf) and the dwell time was 17 s. For the cross sections, the indentations were applied near the centerline of the coating thickness. The reported values of elastic modulus for the coatings were the means of 10 indentations.

3. Results and discussion

3.1. Microstructure of as-sprayed coatings

Fig. 1 presents the polished cross sections of as-sprayed conventional and nanostructured TBCs, which are composed of the YSZ top coat and NiCoCrAlY bond coat deposited on the superalloy substrate by APS process. The fractured cross section morphologies of the conventional and nanostructured YSZ coatings are shown in Figs. 2 and 3 respectively. It can be seen that the microstructure of conventional YSZ coating consists of columnar-grain splats. In contrast, nanostructured YSZ coating exhibits a bimodal microstructure consisting of nanosized particles retained from the non-molten part of powder (nano-zones) and microcolumnar grains formed through the solidification of the melted part of powder. The percentage of nano-zones embedded in the coating structure was approximately 24%. The nano-zones contain a large volume fraction of pores with size ranging from several tens to several hundreds of nanometers.

3.2. Thermal shock behaviors of TBCs

The macroscopic images of the conventional and nanostructured TBCs during thermal shock testing are shown in Fig. 4. As can be seen, for both conventional and nanostructured coatings, starting failure from the edges of the sample occurred and then propagated to the adjacent areas. Beginning of the failure from the edges is due to the extreme heating and cooling conditions encountered and singularity of thermal stresses at the edges. Other

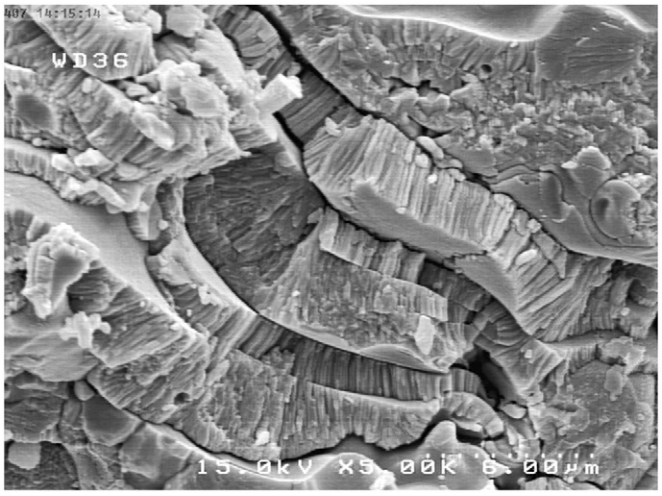

Fig. 2. FESEM micrograph of the fractured cross section of as-sprayed conventional YSZ coating.

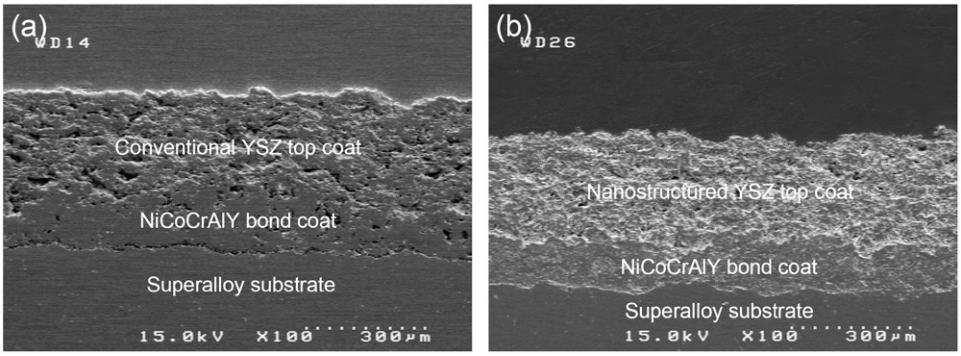

Fig. 1. FESEM micrographs of polished cross section of as-sprayed TBC with conventional YSZ (a) and nanostructured YSZ (b).

studies [24,34,35] have also mentioned the edge effect on failure during the thermal cycling. Fig. 5 presents the weight changes as a function of cycle number for conventional and nanostructured samples during thermal shock testing. Based on this figure, the nanostructured coating, as compared to the conventional one, exhibits a better performance during thermal shock testing. As can be seen, the weight of both samples was first increased due to substrate free surface oxidation and then reduced suddenly after some cycles. After sudden weight loss, a weight gain was observed that can be due to both substrate and bond coat oxidation. Since gradual weight loss was not observed, coatings delamination did not occur. On the other hand, the sudden weight loss of samples implied that coatings spallation could have occurred. The polished cross sections of the conventional and nanostructured TBCs after thermal shock testing are shown in Fig. 6. As can be seen, in both coatings, cracks were initiated within the ceramic top coat near the top coat/bond coat interface. Based on this figure, the lack of thickness loss of both coatings during thermal shock also rejects the coating delamination mechanism. Therefore, the investigation of weight changes graphs (Fig. 5) and microscopic images (Fig. 6) shows that the failure of both nanostructured and conventional YSZ coatings are in a similar mode, and have occurred as spallation of the top coat, near and parallel to the top coat/bond coat interface.

The previous studies [30,36,37] showed that oxidation of the bond coat and thermal mismatch stress were the main factors influencing degradation of TBCs. EDS analyses of top coat/bond coat interfaces of both conventional and nanostructured TBCs after thermal shock testing are shown in Fig. 7. Based on this analysis, for both coatings, thermally grown oxide (TGO) was not formed on the top coat/bond coat interface. The SEM micrographs of samples after thermal shock testing (Fig. 6) also confirm the lack of formation of TGO. Therefore, it can be concluded that bond coat oxidation did not occur during thermal cycling, thereby not contributing to the coating failure. It seems that the lack of visible thickness formation of TGO is due to short heating time. Other studies [24,38] have also pointed to this subject.

Fig. 8 presents the XRD patterns of the as-sprayed and failed YSZ conventional and nanostructured coatings. According to XRD patterns, the as-sprayed coatings were

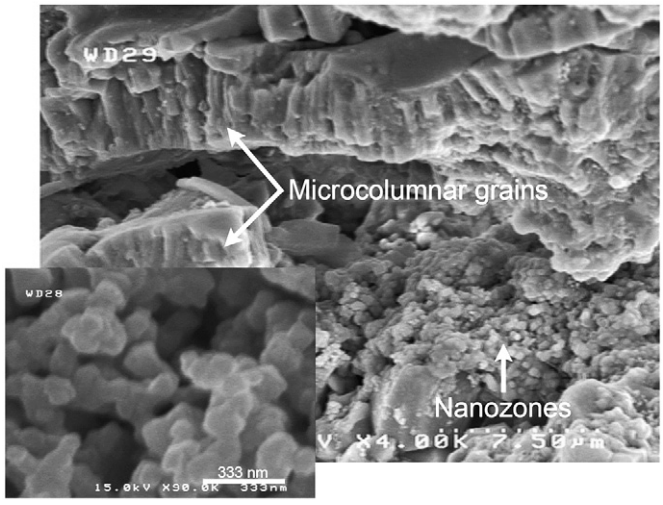

Fig. 3. FESEM micrograph of the fractured cross section of as-sprayed nanostructured YSZ coating (attachment image: non-molten part of powder (nano-zones) within coating at high magnification).

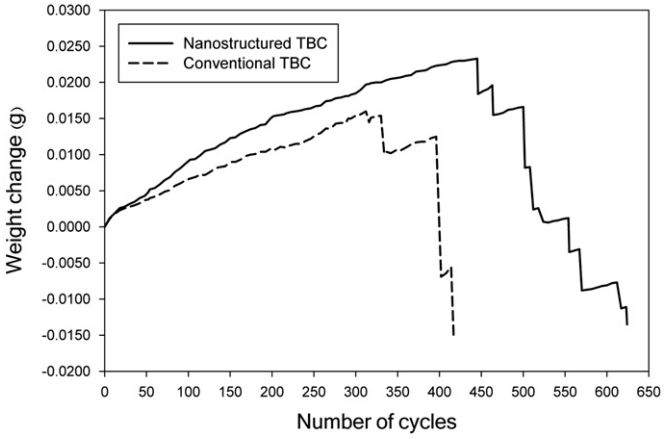

Fig. 5. Weight change as a function of cycle number for conventional and nanostructured TBCs during thermal shock testing.

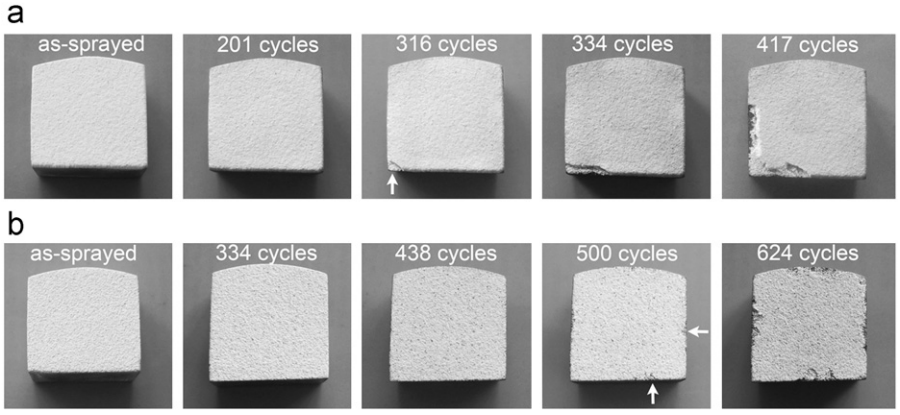

Fig. 4. Photographs of conventional (a) and nanostructured (b) samples during thermal shock testing.

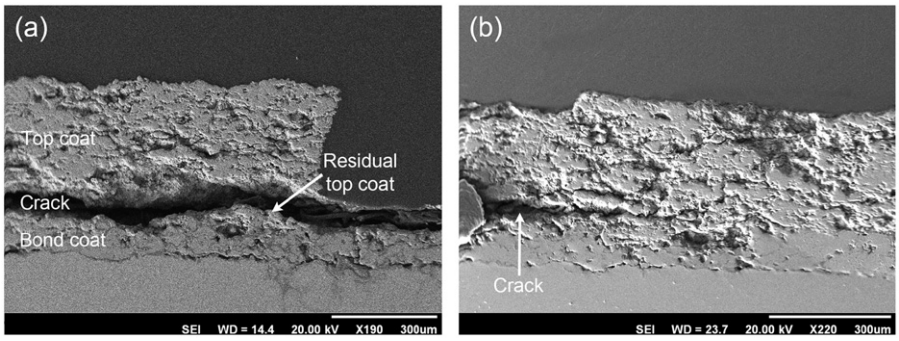

Fig. 6. SEM micrographs of polished cross section of conventional (a) and nanostructured (b) TBCs after 417 and 624 cycles, respectively.

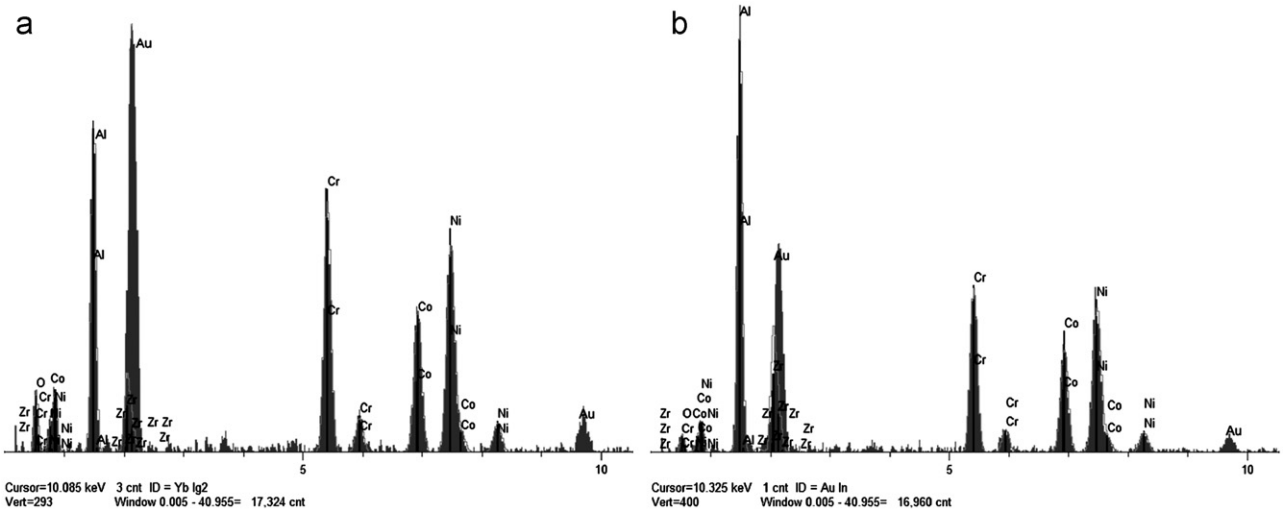

Fig. 7. EDS analyses from top coat/bond coat interface of conventional (a) and nanostructured (b) TBCs after failure.

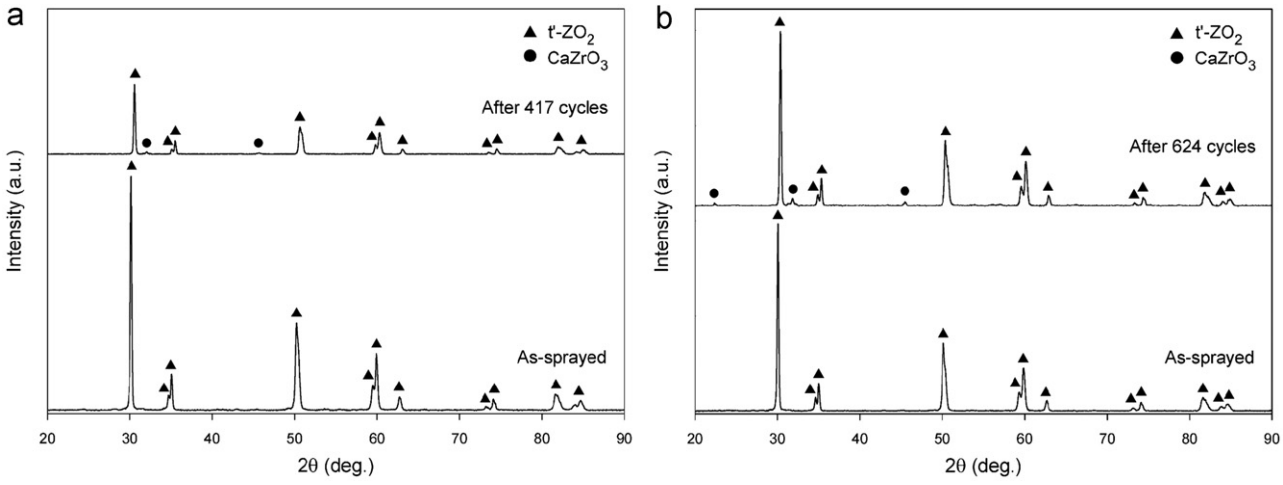

Fig. 8. XRD patterns of conventional (a) and nanostructured (b) YSZ coatings before and after thermal shock testing.

completely made of a non-transformable tetragonal (t′) phase. t′ is the typical phase of plasma-sprayed zirconia, which is formed owing to the quenching of molten droplets during plasma spraying [20,39,40]. The thermally cycled coatings also predominantly contained t′ phase of zirconia with a very small amount of calcium zirconium oxide ($CaZrO_3$). The formation of $CaZrO_3$ can be explained by the observation that the calcium which was present in the tap water reacted with zirconium during the quenching operation [19,41,42]. After long-term thermal cycling, the metastable non-transformable tetragonal phase may be decomposed into the low stabilizer tetragonal phase by the

diffusion of the stabilizer (Y_2O_3), and the low stabilizer tetragonal phase may be transformed to the monoclinic phase. The tetragonal-to-monoclinic phase transformation is martensitic in nature and is accompanied by a significant volume increase of approximately 3–5 vol%, affecting the integrity of the coating [19,43]. Anyway, in this study, no phase change was observed (apart from a very small amount of $CaZrO_3$) during the thermal shock. Accordingly, stresses resulting from phase transformation had no contribution to both coatings degradation.

In layered systems, the coefficient of thermal expansion is an important property because thermal stress resulting from the CTE mismatch between the layers may lead to the degradation. Therefore, CTE mismatch can be one of the key factors responsible for the failure of TBCs. The typical CTE of Inconel 738 Ni-based substrate, plasma-sprayed NiCoCrAlY bond coat, and plasma-sprayed YSZ top coat are reported as $16 \times 10^{-6}\,^{\circ}C^{-1}$ [44,45], $15 \times 10^{-6}\,^{\circ}C^{-1}$ [46] and $10.7 \times 10^{-6}\,^{\circ}C^{-1}$ [44,45], respectively. The substrate and bond coat, due to the relatively same chemical compositions, have low CTE mismatch. But, since the difference in CTE between the ceramic top coat and the underlying metallic components is high, it can be anticipated that top coat/bond coat interface stresses upon heating/cooling of the substrate/coating system are expected to be more. Therefore, thermal stresses caused by the mismatch of the thermal expansion are concentrated on the interface between ceramic top coat and metallic bond coat. With continuous exposure of samples to thermal cycles, these stresses result in crack nucleation and propagation in the ceramic top coat. Later, these initial cracks assisted each other and with propagation in the top coat, near and parallel to top coat/bond coat interface, finally resulted in top coat spallation. Therefore, during thermal shock testing, the failures of both conventional and nanostructured coatings were dominated by thermal stresses generated due to the difference in CTE between the ceramic top coat and the underlying metallic components. Crack formation and propagation in the top coat and remaining little parts of top coat on bond coat (Fig. 6) also confirm this fact.

3.3. Thermal shock lifetime

The thermal cycling lifetimes of the conventional and nanostructured TBCs are graphically presented in Fig. 9. It can be seen that the nanostructured TBC exhibits an excellent average thermal cycling lifetime, approximately 1.5 times higher when compared to the conventional TBC. Lifetime extension of the nanostructured TBC, as compared to the conventional TBC, can be described according to different microstructures of the coatings. Porosities and microcracks improve strain tolerance and durability of coating due to both reduced elastic modulus, hence the low stress value, and stress relaxation [23,43–47].

Fig. 10 shows the elastic modulus values of the plasma-sprayed conventional and nanostructured YSZ coatings.

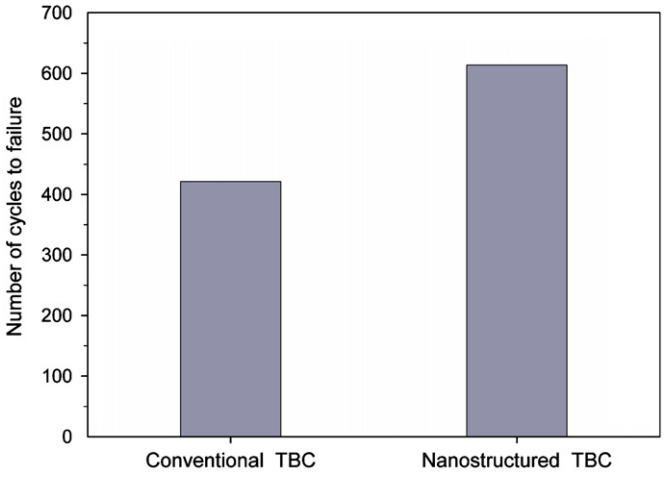

Fig. 9. Thermal cycling lifetime of the conventional and nanostructured TBCs.

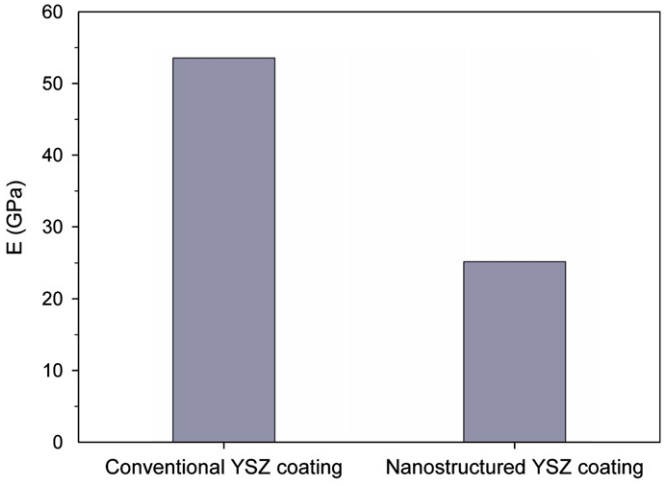

Fig. 10. Elastic modulus of the plasma-sprayed conventional and nanostructured YSZ coatings.

Accordingly, the elastic modulus of the nanostructured coating, as compared to the conventional coating, is much lower. According to Fig. 3, it is possible to observe that the nanostructured YSZ coating, as compared to the conventional YSZ coating, exhibits an extra source of porosity associated with the nano-zones. The presence of this extra source of porosity will cause reduction in the elastic modulus (Fig. 10) and stress relaxation and consequently, increase in the compliance capabilities of the nanostructured coating as compared to its conventional counterpart.

The nanostructured TBCs, as compared to the conventional TBCs, have a higher CTE [48]. Since the CTE of the metallic substrate and bond coat, as compared to the ceramic top coat, are very high, a larger CTE of the top coat means a lower thermal mismatch between the top coat and bond coat layers. Thus, it can be expected that the main factor of TBC failure, i.e., thermal stress generated during the thermal cycling, is lower for nanostructured TBC, as compared to the conventional TBC.

Comparison of weight change curves (Fig. 5) shows that the failure (a destruction of more than 10% in the coating surface) of nanostructured TBC, as compared to the conventional TBC, has occurred in more stages. Based on this, for nanostructured coating, a smaller surface of the coating is degraded in each stage than in the conventional coating. This can be attributed to the ability to control crack propagation in the thermally-sprayed nanostructured coatings [49–51]. In the nanostructured coating with a bimodal microstructure, the splat-boundary structure is periodically interrupted by non-molten parts of powders (nano-zones). Therefore, cracks propagating through splat boundaries are arrested and/or deflected after encountering the nano-zones.

4. Conclusion

In the current study, nanostructured and conventional zirconia based thermal barrier coatings were prepared by atmospheric plasma spraying. Thermal shock test was conducted and the results indicated that the failures of both the nanostructured and conventional TBCs were due to the spallation of top coat, near and parallel to top coat/bond coat interface. Thermal stress caused by the difference in CTE between the ceramic top coat and the underlying metallic components was identified as the major factor of TBC failure. The nanostructured TBC exhibited improved thermal shock resistance as compared to the conventional TBC. The excellent thermal shock resistance of the nanostructured TBC can be attributed to bimodal microstructure container of nano-zones and the existence of extra source of porosity associated with the nano-zones.

Acknowledgments

The authors wish to acknowledge Malek-Ashtar University of Technology for support for this study. The authors would also like to thank Hossein Zamani, Mohsen Jamali, Reza Ghasemi and Zia Valefi for their cooperation.

References

[1] G.D. Girolamo, C. Blasi, M. Schioppa, L. Tapfer, Structure and thermal properties of heat treated plasma sprayed ceria–yttria co-stabilized zirconia coatings, Ceramics International 36 (2010) 961–968.
[2] S. Das, S. Datta, D. Basu, G.C. Das, Thermal cyclic behavior of glass–ceramic bonded thermal barrier coating on nimonic alloy substrate, Ceramics International 35 (2009) 2123–2129.
[3] X. Chen, Y. Zhao, X. Fan, Y. Liu, B. Zou, Y. Wang, H. Ma, X. Cao, Thermal cycling failure of new $LaMgAl_{11}O_{19}$/YSZ double ceramic top coat thermal barrier coating systems, Surface and Coatings Technology 205 (2011) 3293–3300.
[4] N. Wang, C. Zhou, S. Gong, H. Xu, Heat treatment of nanostructured thermal barrier coating, Ceramics International 33 (2007) 1075–1081.
[5] X. Chen, L. Gu, B. Zou, Y. Wang, X. Cao, New functionally graded thermal barrier coating system based on $LaMgAl_{11}O_{19}$/YSZ prepared by air plasma spraying, Surface and Coatings Technology 206 (2012) 2265–2274.
[6] G.D. Girolamo, C. Blasi, L. Pagnotta, M. Schioppa, Phase evolution and thermophysical properties of plasma sprayed thick zirconia coatings after annealing, Ceramics International 36 (2010) 2273–2280.
[7] Y. Li, Y. Xie, L. Huang, X. Liu, X. Zheng, Effect of physical vapor deposited Al_2O_3 film on TGO growth in YSZ/CoNiCrAlY coatings, Ceramics International (2012), http://dx.doi.org/10.1016/j.ceramint.2012.03.014.
[8] S. Das, S. Datta, D. Basu, G.C. Das, Glass–ceramics as oxidation resistant bond coat in thermal barrier coating system, Ceramics International 35 (2009) 1403–1406.
[9] R. Vaßen, M.O. Jarligo, T. Steinke, D.E. Mack, D. Stöver, Overview on advanced thermal barrier coatings, Surface and Coatings Technology 205 (2010) 938–942.
[10] Y. Wang, G. Sayre, Commercial thermal barrier coatings with a double-layer bond coat on turbine vanes and the process repeatability, Surface and Coatings Technology 203 (2009) 2186–2192.
[11] M. Alfano, G.D. Girolamo, L. Pagnotta, D. Sun, Processing, microstructure and mechanical properties of air plasma-sprayed ceria–yttria co-stabilized zirconia coatings, Strain 46 (2010) 409–418.
[12] C.K. Roy, M. Noor-A-Alam, A.R. Choudhuri, C.V. Ramana, Synthesis and microstructure of Gd_2O_3-doped HfO_2 ceramics, Ceramics International 38 (2012) 1801–1806.
[13] Z. Xu, L. He, R. Mu, S. He, X. Zhong, X. Cao, Influence of the deposition energy on the composition and thermal cycling behavior of $La_2(Zr_{0.7}Ce_{0.3})_2O_7$ coatings, Journal of the European Ceramic Society 29 (2009) 1771–1779.
[14] Z. Xu, L. He, R. Mu, X. Zhong, Y. Zhang, J. Zhang, X. Cao, Double-ceramic-layer thermal barrier coatings of $La_2Zr_2O_7$/YSZ deposited by electron beam-physical vapor deposition, Journal of Alloys and Compounds 473 (2009) 509–515.
[15] Z. Xu, L. He, R. Mu, S. He, G. Huang, X. Cao, Double-ceramic-layer thermal barrier coatings based on $La_2(Zr_{0.7}Ce_{0.3})_2O_7$/ $La_2Ce_2O_7$ deposited by electron beam-physical vapor deposition, Applied Surface Science 256 (2010) 3661–3668.
[16] J. Fenech, C. Viazzi, J. Bonino, F. Ansart, A. Barnabe, Morphology and structure of YSZ powders: comparison between xerogel and aerogel, Ceramics International 35 (2009) 3427–3433.
[17] S. Guo, Y. Kagawa, Effect of thermal exposure on hardness and Young's modulus of EB-PVD yttria-partially-stabilized zirconia thermal barrier coatings, Ceramics International 32 (2006) 263–270.
[18] R.W. Steinbrech, V. Postolenko, J. Monch, J. Malzbender, L. Singheiser, Testing method to assess lifetime of EB-PVD thermal barrier coatings on tubular specimens in static and cyclic oxidation tests, Ceramics International 37 (2011) 363–368.
[19] Y. Bai, Z.H. Han, H.Q. Li, C. Xu, Y.L. Xu, Z. Wang, C.H. Ding, J.F. Yang, High performance nanostructured ZrO_2 based thermal barrier coatings deposited by high efficiency supersonic plasma spraying, Applied Surface Science 257 (2011) 7210–7216.
[20] H. Jamali, R. Mozafarinia, R. Shoja Razavi, R. Ahmadi-Pidani, M.R. Loghman-Estarki, Fabrication and evaluation of plasma-sprayed nanostructured and conventional YSZ thermal barrier coatings, Current Nanoscience 8 (3) (2012) 402–409.
[21] W.B. Gong, C.K. Sha, D.Q. Sun, W.Q. Wang, Microstructures and thermal insulation capability of plasma-sprayed nanostructured ceria stabilized zirconia coatings, Surface and Coatings Technology 201 (2006) 3109–3115.
[22] R.S. Lima, B.R. Marple, Toward highly sintering-resistant nanostructured $ZrO_2-7wt\%Y_2O_3$ coatings for TBC applications by employing differential sintering, Journal of Thermal Spray Technology 17 (5–6) (2008) 846–852.
[23] R.S. Lima, B.R. Marple, Y.S.Z. Nanostructured, Thermal barrier coatings engineered to counteract sintering effects, Materials Science and Engineering A 485 (2008) 182–193.
[24] J. Wu, H. Guo, L. Zhou, L. Wang, S.K. Gong, Microstructure and thermal properties of plasma sprayed thermal barrier coatings from nanostructured YSZ, Journal of Thermal Spray Technology 19 (6) (2010) 1186–1194.
[25] B. Liang, C. Ding, Thermal shock resistances of nanostructured and conventional zirconia coatings deposited by atmospheric plasma spraying, Surface and Coatings Technology 197 (2005) 185–192.

[26] C. Liu, Z. Zhang, X. Jiang, M. Liu, Z. Zhu, Comparison of thermal shock behaviors between plasma-sprayed nanostructured and conventional zirconia thermal barrier coatings, Transactions of Nonferrous Metals Society 19 (2009) 99–107.
[27] C. Zhou, N. Wang, H. Xu, Comparison of thermal cycling behavior of plasma-sprayed nanostructured and traditional thermal barrier coatings, Materials Science and Engineering A 452–453 (2007) 569–574.
[28] A.N. Khan, J. Lu, Manipulation of air plasma spraying parameters for the production of ceramic coatings, Journal of Materials Processing Technology 209 (2009) 2508–2514.
[29] L. Wang, Y. Wang, X.G. Sun, J.Q. He, Z.Y. Pan, C.H. Wang, Thermal shock behavior of 8YSZ and double-ceramic-layer $La_2Zr_2O_7$/8YSZ thermal barrier coatings fabricated by atmospheric plasma spraying, Ceramics International (2012), http://dx.doi.org/10.1016/j.ceramint.2011.12.076.
[30] A.N. Khan, J. Lu, Thermal cyclic behavior of air plasma sprayed thermal barrier coatings sprayed on stainless steel substrates, Surface and Coatings Technology 201 (2007) 4653–4658.
[31] K.A. Khor, Y.W. Gu, D. Pan, P. Cheang, Microstructure and mechanical properties of plasma sprayed HA/YSZ/Ti–6Al–4V composite coatings, Biomaterials 25 (2004) 4009–4017.
[32] X. Xie, H. Guo, S. Gong, H. Xu, Lanthanum–titanium–aluminum oxide: a novel thermal barrier coating material for applications at 1300 °C, Journal of The European Ceramic Society 31 (2011) 1677–1683.
[33] Y. Wang, H. Guo, S. Gong, Thermal shock resistance and mechanical properties of $La_2Ce_2O_7$ thermal barrier coatings with segmented structure, Ceramics International 35 (2009) 2639–2644.
[34] R. Ahmadi-Pidani, R. Shoja-Razavi, R. Mozafarinia, H. Jamali, Improving the thermal shock resistance of plasma sprayed CYSZ thermal barrier coatings by laser surface modification, Optics and Lasers in Engineering 50 (2012) 780–786.
[35] C. Giolli, A. Scrivani, G. Rizzi, F. Borgioli, G. Bolelli, L. Lusvarghi, Failure mechanism for thermal fatigue of thermal barrier coating systems, Journal of Thermal Spray Technology 18 (2) (2009) 223–230.
[36] H.L. Tsai, P.C. Tsai, Microstructures and properties of laser-glazed plasma-sprayed ZrO_2–$YO_{1.5}$/Ni–22Cr–10AI–1Y thermal barrier coatings, Journal of Materials Engineering and Performance 4 (1995) 689–696.
[37] Y. Liu, C. Persson, J. Wigren, Experimental and numerical life prediction of thermally cycled thermal barrier coatings, Journal of Thermal Spray Technology 13 (3) (2004) 415–424.
[38] S. Ahmaniemi, P. Vuoristo, T. Mantyla, C. Gualco, A. Bonadei, R.D. Maggio, Thermal cycling resistance of modified thick thermal barrier coatings, Surface and Coatings Technology 190 (2005) 378–387.
[39] R. Ahmadi-Pidani, R. Shoja-Razavi, R. Mozafarinia, H. Jamali, Comparison of hot corrosion resistance of YSZ and CYSZ thermal barrier coatings in presence of sulfate–vanadate molten salts, Advanced Materials Research 472–475 (2012) 141–144.
[40] R.S. Lima, A. Kucuk, C.C. Berndt, Integrity of nanostructured partially stabilized zirconia after plasma spray processing, Materials Science and Engineering A. 313 (2001) 75–82.
[41] Y. Bai, Z.H. Han, H.Q. Li, C. Xu, Y.L. Xu, C.H. Ding, J.F. Yang, Structure–property differences between supersonic and conventional atmospheric plasma sprayed zirconia thermal barrier coatings, Surface and Coatings Technology 205 (2011) 3833–3839.
[42] A.N. Khan, J. Lu, Behavior of air plasma sprayed thermal barrier coatings, subject to intense thermal cycling, Surface and Coatings Technology 166 (2003) 37–43.
[43] S. Bose, High Temperature Coatings, Elsevier Science and Technology Books, Connecticut, USA, 2007.
[44] X. Cao, R. Vassen, D. Stoever, Ceramic materials for thermal barrier coatings, Journal of the European Ceramic Society 24 (2004) 1–10.
[45] R. Vaßen, G. Kerkhoff, D. Stöver, Development of a micromechanical life prediction model for plasma sprayed thermal barrier coatings, Materials Science and Engineering A 303 (2001) 100–109.
[46] Y. Liu, C. Persson, S. Melin, J. Wigren, Long crack behavior in a thermal barrier coating upon thermal shock loading, Journal of Thermal Spray Technology 14 (2) (2005) 258–263.
[47] R. Vaßen, F. Traeger, D. Stöver, Correlation between spraying conditions and microcrack density and their influence on thermal cycling life of thermal barrier coatings, Journal of Thermal Spray Technology 13 (3) (2004) 396–404.
[48] H. Chen, X. Zhou, C. Ding, Investigation of the thermomechanical properties of a plasma-sprayed nanostructured zirconia coating, Journal of the European Ceramic Society 23 (2003) 1449–1455.
[49] R.S. Lima, B.R. Marple, Thermal spray coatings engineered from nanostructured ceramic agglomerated powders for structural, thermal barrier and biomedical applications: a review, Journal of Thermal Spray Technology 16 (1) (2007) 40–63.
[50] M. Gell, E.H. Jordan, Y.H. Sohn, D. Goberman, L. Shaw, T.D. Xiao, Development and implementation of plasma sprayed nanostructured ceramic coatings, Surface and Coatings Technology 146-147 (2001) 48–54.
[51] R.S. Lima, B.R. Marple, Enhanced ductility in thermally sprayed titania coating synthesized using a nanostructured feedstock, Materials Science and Engineering A. 395 (2005) 269–280.